HHS Public Access

Author manuscript

Angew Chem Int Ed Engl. Author manuscript; available in PMC 2024 August 01.

Published in final edited form as:

Angew Chem Int Ed Engl. 2023 August 01; 62(31): e202300467. doi:10.1002/anie.202300467.

Variations in Intracellular Organometallic Reaction Frequency Captured by Single-Molecule Fluorescence Microscopy

Dat Nguyen[a], **Guangjie Yan**[b], **Tai-Yen Chen**[b], **Loi H. Do**[b]

[a]Faculty of Chemical and Food Technology, Ho Chi Minh City University of Technology and Education, 1 Vo Van Ngan, Thu Duc City, Ho Chi Minh City, Vietnam

[b]Department of Chemistry, University of Houston, 4800 Calhoun Rd, Houston, Texas 77004, United States

Abstract

Studies of organometallic reactions in living cells commonly rely on ensemble-averaged measurements, which can obscure the detection of reaction dynamics or location-specific behavior. This information is necessary to guide the design of bioorthogonal catalysts with improved biocompatibility, activity, and selectivity. By leveraging the high spatial and temporal resolution of single-molecule fluorescence microscopy, we have successfully captured single-molecule events promoted by Ru complexes inside live A549 human lung cells. By observing individual allylcarbamate cleavage reactions in real-time, our results revealed that they occur with greater frequency inside the mitochondria than in the non-mitochondria regions. The estimated turnover frequency of the Ru complexes was at least 3-fold higher in the former than the latter. These results suggest that organelle specificity is a critical factor to consider in intracellular catalyst design, such as in developing metallodrugs for therapeutic applications.

Graphical Abstract

tchen37@central.uh.edu; loido@uh.edu, Social Media Twitter handle: @DoResearchGroup (for Do research group).

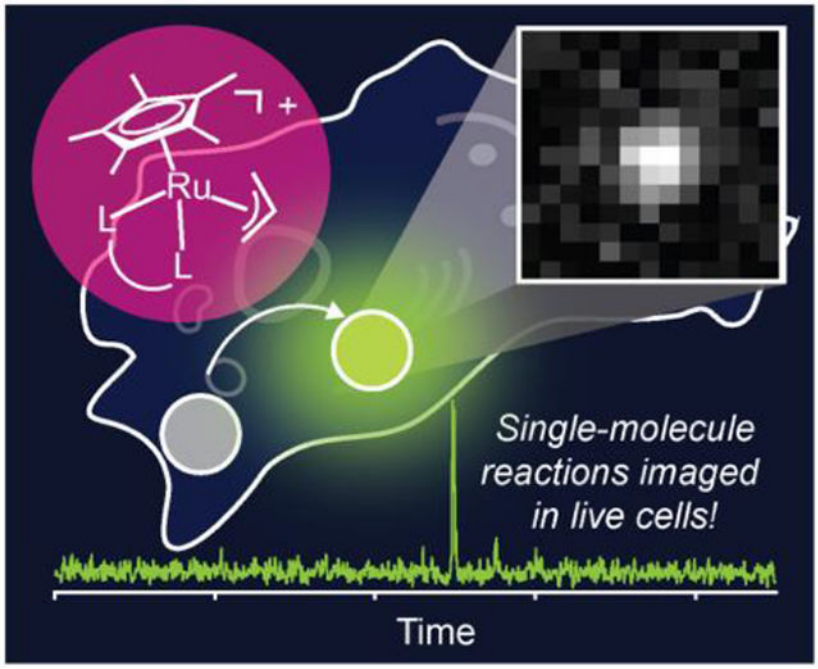

Single-molecule fluorescence microscopy was used to quantify ruthenium-promoted allylcarbamate cleavage reactions in live A549 human lung cells. Individual turn-on events were detected as single fluorescence spots and found to occur more frequently in the mitochondria than the rest of the cell. These results suggest that the subcellular distribution is an important consideration in designing intracellular catalysts.

Keywords

bioorthogonal; bioorganometallic; intracellular catalysis; ruthenium; allylcarbamate cleavage

Introduction

Bioorthogonal chemistry has played important roles in advancing the life sciences, ranging from biomedical imaging to targeted therapeutics.[1-5] Although metal-free click reactions are powerful tools in the biosynthetic chemistry arsenal, processes mediated by metal complexes (e.g., small molecule intracellular metal catalysts[6] or nanozymes[7-8]) offer additional capabilities and opportunities for catalytic amplification.[6, 9-12] A variety of organometallic catalysts have been developed to promote new-to-nature reactions, including C—C bond cross-coupling,[13] olefin metathesis,[14-15] protecting group cleavage,[16] ring formation,[17-18] and transfer hydrogenation.[19-21] Among these, the use of metal-catalyzed allylcarbamate cleavage reactions is growing in popularity (Scheme 1),[10, 22-24] providing a convenient method to uncage bioactive agents (e.g., essential nutrients, anti-cancer drugs, or DNA intercalators) in vitro and in vivo. Research in bioorthogonal catalysis could lead to the discovery of new ways to interface with living systems or combat diseases.

Although organometallic catalysts have been shown to be active inside living systems, quantitative information about their intracellular distribution and activity is generally lacking.[25] Typically, assays are performed at the ensemble level to confirm catalysis in cells, such as using fluorogenic substrates that turn on only after undergoing a desired transformation. Although they are effective for qualitative monitoring of intracellular reactions, these assays cannot offer insights into the catalytic efficiency or organelle specificity.

A recent report by Mascareñas and coworkers provided evidence of organometallic reaction turnover in cells by combining measurements from liquid chromatography-mass spectrometry (LC-MS), which quantified total product formation, and inductively-coupled plasma mass spectrometry (ICP-MS), which quantified catalyst uptake.[26] In work by Cai and coworkers,[27] the reaction yields of azide-alkyne cycloaddition reactions inside cells were estimated based on LC-MS measurements. Although these studies represent an important step toward making intracellular catalysis development more rigorous, they rely on ensemble-averaged measurements (i.e., using results obtained from whole cell populations and different cell samples). Because the intracellular environment is heterogenous and individual cells can differ from one another, critical data concerning the catalyst's reaction dynamics or location-specific behavior are lost.[28-29] Without this information, efforts to design more efficient and selective intracellular catalysts will have a lower likelihood of success.

To perform in-depth analyses of metal-promoted reactions inside living cells, we used single-molecule fluorescence microscopy (SMFM)[30-33] to track allylcarbamate cleavage reactions in real-time. Because SMFM is capable of imaging with high spatial and temporal resolution, we can determine precisely where and when single-molecule events take place, respectively. SMFM has been applied to interrogate key biological processes[34-39] but, to the best of our knowledge, has not been used to study organometallic reactions in cells.[40-43] In this work, we demonstrate that SMFM is well suited for quantitative visualization of metal-promoted processes in living systems,[43] providing insights previously unattainable using conventional approaches. Fundamental questions regarding the location of metal-promoted reactions, turnover frequency (TOF),[44] and environment-dependent reactivity were investigated. Because living systems are highly complex, our results suggest that using tools capable of providing subcellular information is necessary for quantitative studies of in-cell catalysis.

Results and Discussion

Reactions in Solution

The bioorthogonal conversion of allylcarbamates to amines in living systems can be mediated by a variety of ruthenium[10, 22, 45] and iridium[46] catalysts. Initially, we screened both Ru(II) and Ru(IV) complexes for their catalytic activity by combining *N*-allyloxycarbonyl-4-chloroaniline with 5 mol% of a Ru complex and excess thiophenol in methanol at room temperature (Table S1). NMR spectroscopic analysis of the reaction products revealed that >99% yield of 4-chloroaniline was obtained using [Ru^{II}(Cp*)(COD)Cl] (**Ru1,** Cp* = pentamethylcyclopentadienyl anion, COD = 1,5-cyclooctadiene),

$[Ru^{II}(Cp^*)(PPh_3)_2Cl]$ (**Ru2**), $[Ru^{IV}(Cp^*)$(2-quinolinecarboxylate)(allyl)$]PF_6$ (**Ru3**), $[Ru^{IV}(Cp^*)$(8-hydroxyquinolinate)(allyl)$]PF_6$ (**Ru4**), $[Ru^{II}(Cp^*)(CH_3CN)_3]PF_6$ (**Ru5**), and $[Ru^{IV}(Cp^*)(allyl)Cl_2]$ (**Ru6**). In contrast, $[Ru^{II}$(*p*-cymene)(picolinamidate)Cl (**Ru7**) and $[Ru^{II}$(hexamethylbenzene)(2,2′-bipyridine)Cl]Cl (**Ru8**) were inactive.

Next, we performed kinetic studies of allylcarbamate cleavage reactions in different aqueous media using fluorescence spectroscopy (Figure 1). Mixtures containing fluorogenic substrate **1** (40 μM), thiophenol (200 μM), and Ru complex (2 μM) were added to individual wells in 24-well plates and the fluorescence changes were monitored over time at 522 nm using a microplate reader.[22] Because conversion of the allyloxycarbonyl-protected substrate **1** led to the formation of the highly emissive rhodamine 110 (compound **2**), the reaction yields could be calculated using the fluorescence intensity observed. We found that the Ru(II) complexes (i.e., **Ru1** and **Ru2**) in phosphate-buffered saline (PBS) achieved greater than 65% yield in 10 min, whereas the Ru(IV) complexes (i.e., **Ru3** and **Ru4**) required at least 50 min to afford the same amount. Because Ru(IV)-allyl species must be converted to the corresponding Ru(II) form prior to reacting with substrates (Scheme S1),[10] **Ru3**/**Ru4** is expected to have a slower initial rate than **Ru1**/**Ru2**. In separate but related work,[45] Meggers and coworkers found that reducing the steric bulk of the Ru(IV) complexes by using unsubstituted cyclopentadienyl anion instead of Cp* enhanced their rates relative to that of **Ru1** in potassium phosphate-buffered solutions. Thus, these results suggest that the activity of the Ru complexes is highly tunable.

When kinetic measurements were conducted in complex aqueous media, the Ru catalyst activity generally decreased in the order PBS > cell lysate > Dulbecco's Modified Eagle Medium (DMEM) > DMEM/fetal bovine serum (FBS) (Figure 1B). This trend tracks with the presence of increasing amounts of nucleophilic components in the media, which could potentially deactivate the Ru complexes. FBS, which contains an undefined mixture of growth factors, proteins, metal salts, vitamins, and hormones, is most poorly tolerated by **Ru1**-**Ru3**. The Ru(II) species are more susceptible to coordinative inhibition than the Ru(IV) species, resulting in the activity trend **Ru4** > **Ru3** > **Ru2** ≈ **Ru1** in DMEM/FBS, which differs from that observed in PBS. These results are relevant to living systems because the cellular environment comprises a plethora of species that could potentially poison the Ru complexes.[47]

Biocompatibility of the Ru Complexes

Before carrying out allylcarbamate cleavage reactions in cells, we first investigated the biocompatibility of the Ru complexes. Their tolerable concentrations were measured using tetrazolium-based cell viability assays. Our results showed that A549 human lung cells can be treated with at least 20 μM or higher concentrations of **Ru1**, **Ru2**, or **Ru3** for 4 h without adverse biological effects (Figures S7-S9). **Ru4** exhibited a lower tolerable concentration, achieving >95% cell viability only when cells were exposed to less than 10 μM of the complex within the same time period. Knowing these limits allowed us to determine suitable amounts of **Ru1**-**Ru4** to use in our SMFM imaging studies below. As a reference point, other reports on ruthenium catalysis in cells have employed Ru concentrations of 2-40 μM in various mammalian cells without causing cell death.[10, 22, 24, 48]

To measure cellular uptake, we treated A549 cells with 1 μM of the Ru complexes for 2 h and then analyzed the samples for Ru abundance by ICP-MS (Figure 2, Table S2). We found that cells incubated with **Ru2**, **Ru3**, and **Ru4** contained 0.4×10^{-16}, 4.1×10^{-16}, and 1.6×10^{-16} g of Ru per cell, respectively (Figure 2). The Ru concentration in the **Ru1** sample was below the instrument detection limit. Increasing the **Ru1** and **Ru2** treatment amount to 20 μM led to a corresponding increase in Ru uptake, with intracellular concentrations of 6.0×10^{-16} and 4.4×10^{-16} g of Ru per cell, respectively. Based on the cell viability and accumulation results, **Ru1**-**Ru4** were deemed sufficiently biocompatible for live cell imaging studies.

Reactions in Individual Cells

To identify conditions suitable for imaging using SMFM, we first carried out experiments in pure water. An aqueous solution containing **Ru1** (1 μM), probe **1** (10 nM), and PhSH (1 μM) was added to a custom-made single-well slide. The mixture was excited continuously using a 488 nm laser and fluorescence images at 525 nm were acquired at a speed of 10 frames/s (fps) for 100 s (Figure 3A). The amount of **1** present was kept in the nanomolar range to ensure that the formation of **2** could be observed as individual fluorescent spots. These events are likely due to Ru-promoted cleavage of **1** to **2**, followed by photobleaching of **2**. As shown in Figure 3A, solutions containing **Ru1**, **1**, and PhSH produced about 1000 single-molecule events, which was significantly higher than that observed in control samples lacking the Ru complex, probe, or thiol (≤ 67 spots). Additionally, the fluorescence intensities of spots observed in the **Ru1**/**1**/PhSH wells were significantly higher than those in the control (Figure S22), indicating that the emission turn on events resulted from allylcarbamate cleavage rather than background fluorescence.

Once our SMFM imaging method was optimized, we investigated Ru-promoted uncaging reactions in live A549 cells. In a typical experiment, cells in single-well slides were incubated with a Ru complex for 2 h, washed with fresh media, and then treated with **1** for 30 min (Figure 3B). The samples were first irradiated with a 488 nm laser for 25 s to photobleach any molecules of **2** formed during incubation. Fluorescence images were then acquired for 100 s under continuous laser exposure, which clearly showed individual spots appearing randomly due to the formation of **2**.[22] In biological systems, the diffusion rate of molecules is typically on the order of 1-10 $\mu m^2/s$. These results suggest that the diffusion of **2** inside cells is slow enough to be captured by our microscope camera, which has a time resolution of 0.1 s. Reversing the order of addition by treating A549 cells with **1** first before incubating with the Ru complex was not suitable for single-molecule imaging because the conversion of **1** to **2** was too rapid, causing oversaturation of the fluorescence signals and precluding individual spot detection (Figure S13). By filtering the images through a cell mask (Figure S17), we were able to distinguish whether a reaction took place inside or outside the cell. As shown in Figure 3B (bottom left), greater number of single-molecule spots were detected in samples containing both **Ru1** (20 μM) and **1** (20 μM) (PhSH is not needed in cell studies due to the presence of endogenous thiols) than in the untreated or **Ru1** only treated controls. The area spot frequency, which is determined by dividing the total spot count over the imaging area per second, varied widely from cell to cell, even between those in the same sample well (Figure 3B, top). This variability may result from differences

in the accumulation of **Ru1** and **1** or the extent of deactivation within individual cells. Importantly, the area spot frequency was about 5-fold higher inside than outside the cell (2.0×10^{-2} vs. 0.4×10^{-2} spot/μm^2·s, respectively), confirming that Ru-promoted reactions were predominantly intracellular. It is possible that the extracellular spots could arise from the transport of **2** from inside to outside the cell.

Detailed analysis of the single-molecule images revealed that most fluorescence spots lasted for <0.2 s in cells (Figure S15). Some spots were due to single events (Figure 4A, top), whereas others represented multiple events (bottom). The latter may result from sequential uncaging reactions promoted by the same Ru molecule. However, because the Ru species could diffuse freely inside the cell, we cannot dismiss the possibility that fluorescent spots occurring in succession were generated by different Ru complexes. The microscope objective's depth of focus is more narrow than the length of the cell,[49] so not all Ru-promoted reactions could be captured (Figure 4B). Thus, a turn-on event is the result of either an uncaging reaction induced by the Ru complex (path i) or diffusion of **2** into the imaging window (path ii). Because the cells were illuminated for 25 s prior to data collection, the early frames should be devoid of any pre-existing **2** due to light-induced degradation within the imaging window. Meanwhile, the turn-off events may result from out-of-view diffusion (path iii) or photobleaching to generate non-emissive species **3** (path iv). Based on control studies, the diffusion of **2** in and out of the imaging window has a negligible contribution to the total spot count (Figure S24B).

We next assessed the area spot frequency of allylcarbamate cleavage reactions for the entire Ru series. Because the Ru(II) complexes (i.e., **Ru1** and **Ru2**) are less active than the Ru(IV) complexes (i.e., **Ru3** and **Ru4**), greater amounts of the former relative to the latter were needed to obtain meaningful single-molecule data. After screening different Ru concentrations, we found that using 20 μM of **Ru1**/**Ru2** and 1 μM of **Ru3**/**Ru4** with the corresponding amounts of **1** were needed to obtain sufficient single fluorescence spots for statistically significant analyses. In experiments containing **Ru3** and **Ru4**, the 30 min incubation step with **1** was omitted to prevent the formation of too many molecules of **2** prior to imaging. Our results showed that the spot frequencies varied from 4.3×10^{-2} to 9.6×10^{-2} spot/μm^2·s. Once again, significant variability between individual cells in the same sample well was observed (Figures 3B and S25-S28).

The turnover frequency (TOF) of the in-cell reactions was estimated by dividing the area spot frequency over the Ru concentration. Because the Ru content in the SMFM imaged cells could not be obtained directly (i.e., the Ru complexes are non-emissive), it was acquired from ICP-MS measurements of separate cell samples. Thus, the TOF values calculated are ensemble-averaged. Based on this analysis, we found that the Ru complexes exhibited TOFs in the order **Ru4** (1.3×10^{-4} s^{-1}) > **Ru3** (1.1×10^{-4} s^{-1}) > **Ru2** (6.6×10^{-5} s^{-1}) > **Ru1** (1.6×10^{-5} s^{-1}) (Figure S29). This trend is consistent with that observed in uncaging reactions performed in non-PBS aqueous mixtures (Table S5). However, the activity differences between **Ru1** and **Ru2** were significantly greater in live cells ($TOF_{\mathbf{Ru2}}$/$TOF_{\mathbf{Ru1}}$ = 4.2) than in solution ($TOF_{\mathbf{Ru2}}$/$TOF_{\mathbf{Ru1}}$ = 1.0–1.3) (Figure S30A). In contrast, **Ru3** and **Ru4** showed similar relative activities in cells ($TOF_{\mathbf{Ru4}}$/$TOF_{\mathbf{Ru3}}$ = 1.2) and in solution ($TOF_{\mathbf{Ru2}}$/$TOF_{\mathbf{Ru1}}$ = 1.0-2.1) (Figure S30B). We hypothesize that because the Ru(II)

complexes are more substitutionally labile than Ru(IV) complexes, they are more sensitive to the variable composition of the intracellular matrix. Thus, although studies performed in aqueous media can provide useful information about reactions in cells, they cannot adequately capture the complexity of living systems.

To interrogate the behavior of individual Ru complexes, they should be fluorescently labeled and immobilized so that the origin of each uncaging event could be tracked.[42, 50] Because our Ru complexes are non-emissive and can diffuse freely in solution, it was not possible in the current study to assess whether they achieved turnover inside the cell. Despite this limitation, our results showed unambiguously that individual organometallic reactions could be detected inside living environments, demonstrating that SMFM is a powerful tool for real-time tracking of intracellular processes.

Reactions in the Mitochondria

Half-sandwich metal complexes can localize in different cellular organelles to different extents.[51-54] Because the local cell environment can differ in pH, viscosity, redox potential, and other factors,[55-56] we hypothesized that the Ru complexes could exhibit variability in their intracellular behavior. Based on reports that some Ru species have high affinity for the mitochondria,[53] we performed SMFM experiments on A549 cells stained with the commercial mitochondria dye MitoTracker Deep Red (MTDR). Cells were incubated with **Ru3** or **Ru4** (1 μM) and MTDR for 2 h, followed by the addition of **1** (1 μM), and then dual-color images were acquired continuously for 100 s. In the 680 nm channel (Figure 5A), strong red fluorescence was observed, revealing the location of the mitochondria inside the cell. Using these images, mitochondrial masks were constructed so that the fluorescent spots appearing in the 525 nm channel due to the formation of **2** could be sorted based on their locations. Our results revealed that, on average, cells treated with either **Ru3** or **Ru4** displayed more single-molecule events inside the mitochondria than non-mitochondria regions, which include the cytosol and other organelles (Figure 5B and S31). A variety of reasons could account for these observations. For example, it is possible that the Ru complexes accumulate more in the mitochondria than the rest of the cell, exhibit environment-specific behavior, and/or are deactivated to different degrees inside the cell.

To assess the possibilities above, further studies were conducted to quantify the amount of Ru complexes in different cellular compartments. Because **Ru3** and **Ru4** are non-emissive, their concentrations were estimated indirectly based on separate ICP-MS measurements rather than directly via SMFM imaging. Using a commercial cell fractionation kit (see Section V in the SI), we separated the mitochondria from the cytosol in A549 cells pre-incubated with the Ru complexes and measured the amount of Ru in each fraction. During the isolation process, the nuclei and cell debris were discarded so the Ru content measured may not represent the total amount in cells. Keeping this caveat in mind, our results showed that only ~3% of the Ru detected was in the mitochondria whereas ~97% was in the cytosol (Figure 5C, left, and Table S3). Based on these data, the ensemble-averaged TOFs for the Ru complexes were calculated. The estimated non-mitochondria TOFs are upper limits because the amount of Ru in the nucleus and cell debris was not included in the ICP-MS measurements. As shown in Figure 5C (right), **Ru3** and **Ru4** exhibited about

3.1- and 3.7-fold increases in TOF in the mitochondria vs. cytosol, respectively. Because the Ru content in the cytosol is significantly higher than in the mitochondria, it is likely that a high percentage of **Ru3** and **Ru4** in the cytosol exists in an inactive state, potentially due to coordinative inhibition by biomolecules. At this time, we cannot dismiss other possibilities, such as differences in local pH that can alter the allylcarbamate cleavage reaction rates in different subcellular locations. Additionally, there could be environment-specific factors that affect fluorophore photophysics and diffusion rates, but such effects were found to be negligible in our studies (Figure S23). These results are significant because they provide evidence of reaction heterogeneity within individual cells, a phenomenon that could not be captured previously using conventional imaging techniques (e.g., confocal laser scanning microscopy).

Conclusion

We demonstrate unambiguously that organometallic reactions could be promoted by synthetic metal complexes inside living cells. Using SMFM, we determined precisely when and where individual allylcarbamate cleavage reactions took place by tracking single-molecule events induced by uncaging fluorogenic substrates. Qualitatively, the activity of the Ru complexes in the cell (i.e., **Ru4** > **Ru3** > **Ru2** > **Ru1**) mirrors that observed in DMEM or DMEM/FBS, although their relative differences could vary significantly in cells vs. in solution. By staining A549 cells with MTDR, we were able to quantify the number of allylcarbamate cleavage reactions occurring in the mitochondria vs. non-mitochondria compartments. Although the total spot counts varied between cells, it was clear that the uncaging events occurred more frequently in the mitochondria. The ensemble-averaged TOFs, calculated by combining SMFM and ICP-MS data, suggest that the conversion of **1** to **2** by Ru complexes was at least 3-fold higher in the mitochondria than in the cytosol. This observation could be due to a variety of factors, such as differences in the relative distribution of active vs. inactive Ru species inside the cell and/or environment-specific effects on the reaction. Further investigations are needed to track individual catalyst molecules using SMFM and assess whether they achieve reaction turnover.

This work suggests that current tools used to study intracellular catalysis are inadequate because ensemble averaging obscures important information about reaction dynamics and heterogeneity within the cell interior. Understanding a catalyst's intracellular behavior will allow researchers to design variants with improved efficiency and selectivity. For example, a mitochondria-targeted catalyst could be used to treat mitochondria dysfunction associated with neurodegenerative[57-58] or cardiovascular diseases.[59-60] We anticipate that our SMFM imaging methods could be readily applied to study other organometallic reactions in cells, paving the way for the development of new biorthogonal chemistry or catalytic metallodrugs.

Supplementary Material

Refer to Web version on PubMed Central for supplementary material.

Acknowledgements

The authors are grateful to the Welch Foundation (Grant No. E-1894 to L.H.D.) and the National Institutes of Health (Grant No. R01GM129276 to L.H.D. and R35GM133505 to T.-Y. C.) for funding this work.

References

[1]. Sletten EM, Bertozzi CR, Angew. Chem. Int. Ed 2009, 48, 6974–6998.

[2]. Sletten EM, Bertozzi CR, Acc. Chem. Res 2011, 44, 666–676. [PubMed: 21838330]

[3]. Taiariol L, Chaix C, Farre C, Moreau E, Chem. Rev 2022, 122, 340–384. [PubMed: 34705429]

[4]. Wu D, Yang K, Zhang Z, Feng Y, Rao L, Chen X, Yu G, Chem. Soc. Rev 2022, 51, 1336–1376. [PubMed: 35050284]

[5]. Battigelli A, Almeida B, Shukla A, Bioconjugate Chem. 2022, 33, 263–271.

[6]. Ngo AH, Bose S, Do LH, Chem.-Eur. J 2018, 24, 10584–10594. [PubMed: 29572980]

[7]. Wei H, Wang E, Chem. Soc. Rev 2013, 42, 6060–6093. [PubMed: 23740388]

[8]. Zhou Y, Liu B, Yang R, Liu J, Bioconjugate Chem. 2017, 28, 2903–2909.

[9]. Seoane A, Mascareñas JL, Eur. J. Org. Chem 2022, e202200118.

[10]. Völker T, Dempwolff F, Graumann PL, Meggers E, Angew. Chem. Int. Ed 2014, 53, 10536–10540.

[11]. Soldevila-Barreda JJ, Metzler-Nolte N, Chem. Rev 2019, 119, 829–869. [PubMed: 30618246]

[12]. Soldevila-Barreda JJ, Sadler PJ, Curr. Opin. Chem. Biol 2015, 25, 172–183. [PubMed: 25765750]

[13]. Li N, Lim RKV, Edwardraja S, Lin Q, J. Am. Chem. Soc 2011, 133, 15316–15319. [PubMed: 21899368]

[14]. Toussaint SNW, Calkins RT, Lee S, Michel BW, J. Am. Chem. Soc 2018, 140, 13151–13155. [PubMed: 30281288]

[15]. Binder JB, Raines RT, Curr. Opin. Chem. Biol 2008, 12, 767–773. [PubMed: 18935975]

[16]. Li J, Chen PR, Nat. Chem. Biol 2016, 12, 129–137. [PubMed: 26881764]

[17]. Miguel-Ávila J, Tomás-Gamasa M, Mascareñas JL, Angew. Chem. Int. Ed 2020, 59, 17628–17633.

[18]. Vong K, Yamamoto T, Chang T.-c., Tanaka K, Chem. Sci 2020, 11, 10933–10938.

[19]. Bose S, Ngo AH, Do LH, J. Am. Chem. Soc 2017, 139, 8792–8795. [PubMed: 28613857]

[20]. Coverdale JPC, Romero-Canelón I, Sanchez-Cano C, Clarkson GJ, Habtemariam A, Wills M, Sadler PJ, Nat. Chem 2018, 10, 347–354. [PubMed: 29461524]

[21]. Banerjee S, Sadler PJ, RSC Chem. Biol 2021, 2, 12–29. [PubMed: 34458774]

[22]. Streu C, Meggers E, Angew. Chem. Int. Ed 2006, 45, 5645–5648.

[23]. Lee Y, Umeano A, Balskus EP, Angew. Chem. Int. Ed 2013, 52, 11800–11803.

[24]. Sánchez MI, Penas C, Vázquez ME, Mascareñas JL, Chem. Sci 2014, 5, 1901–1907. [PubMed: 25632343]

[25]. Nguyen DP, Nguyen HTH, Do LH, ACS Catal. 2021, 11, 5148–5165. [PubMed: 34824879]

[26]. Vidal C, Tomás-Gamasa M, Gutiérrez-González A, Mascareñas JL, J. Am. Chem. Soc 2019, 141, 5125–5129. [PubMed: 30892889]

[27]. Li S, Wang L, Yu F, Zhu Z, Shobaki D, Chen H, Wang M, Wang J, Qin G, Erasquin UJ, Ren L, Wang Y, Cai C, Chem. Sci 2017, 8, 2107–2114. [PubMed: 28348729]

[28]. Liu Z, Lavis LD, Betzig E, Mol. Cell 2015, 58, 644–659. [PubMed: 26000849]

[29]. Rissin DM, Gorris HH, Walt DR, J. Am. Chem. Soc 2008, 130, 5349–5353. [PubMed: 18318491]

[30]. Lelek M, Gyparaki MT, Beliu G, Schueder F, Griffié J, Manley S, Jungmann R, Sauer M, Lakadamyali M, Zimmer C, Nat. Rev. Method Primers 2021, 1, 39.

[31]. Sahl SJ, Hell SW, Jakobs S, Nat. Rev. Mol. Cell Biol 2017, 18, 685–701. [PubMed: 28875992]

[32]. Stephens DJ, Allan VJ, Science 2003, 300, 82–86. [PubMed: 12677057]

[33]. Patterson G, Davidson M, Manley S, Lippincott-Schwartz J, Annu. Rev. Phys. Chem 2010, 61, 345–367. [PubMed: 20055680]

[34]. Jung W, Sengupta K, Wendel BM, Helmann JD, Chen P, Nucleic Acids Res. 2020, 48, 2199–2208. [PubMed: 32009151]

[35]. Chen T-Y, Cheng Y-S, Huang P-S, Chen P, Acc. Chem. Res 2018, 51, 860–868. [PubMed: 29368512]

[36]. Zhao ZW, Roy R, Gebhardt JCM, Suter DM, Chapman AR, Xie XS, Proc. Natl. Acad. Sci. U.S.A 2014, 111, 681–686. [PubMed: 24379392]

[37]. Chong S, Chen C, Ge H, Xie XS, Cell 2014, 158, 314–326. [PubMed: 25036631]

[38]. Cheng X, Chen K, Dong B, Yang M, Filbrun SL, Myoung Y, Huang T-X, Gu Y, Wang G, Fang N, Nat. Cell Biol 2021, 23, 859–869. [PubMed: 34253896]

[39]. Chen K, Gu Y, Sun W, Bin D, Wang G, Fan X, Xia T, Fang N, Nat. Commun 2017, 8, 887. [PubMed: 29026088]

[40]. Easter QT, Blum SA, Acc. Chem. Res 2019, 52, 2244–2255. [PubMed: 31310095]

[41]. Easter QT, Blum SA, Angew. Chem. Int. Ed 2018, 57, 1572–1575.

[42]. Easter QT, Blum SA, Angew. Chem. Int. Ed 2017, 56, 13772–13775.

[43]. Halabi EA, Thiel Z, Trapp N, Pinotsi D, Rivera-Fuentes P, J. Am. Chem. Soc 2017, 139, 13200–13207. [PubMed: 28820941]

[44]. Roeffaers MBJ, Sels BF, Uji-i H, De Schryver FC, Jacobs PA, De Vos DE, Hofkens J, Nature 2006, 439, 572–575. [PubMed: 16452976]

[45]. Völker T, Meggers E, ChemBioChem 2017, 18, 1083–1086. [PubMed: 28425643]

[46]. Singh N, Gupta A, Prasad P, Mahawar P, Gupta S, Sasmal PK, Inorg. Chem 2021, 60, 12644–12650. [PubMed: 34392682]

[47]. Wilson YM, Dürrenberger M, Nogueira ES, Ward TR, J. Am. Chem. Soc 2014, 136, 8928–8932. [PubMed: 24918731]

[48]. Sasmal PK, Carregal-Romero S, Parak WJ, Meggers E, Organometallics 2012, 31, 5968–5970.

[49]. Jiang R-D, Shen H, Piao Y-J, Rom. J. Morphol. Embryol 2010, 51, 663–667. [PubMed: 21103623]

[50]. Esfandiari NM, Wang Y, Bass JY, Cornell TP, Otte DAL, Cheng MH, Hemminger JC, McIntire TM, Mandelshtam VA, Blum SA, J. Am. Chem. Soc 2010, 132, 15167–15169. [PubMed: 20731349]

[51]. Conesa JJ, Carrasco AC, Rodríguez-Fanjul V, Yang Y, Carrascosa JL, Cloetens P, Pereiro E, Pizarro AM, Angew. Chem. Int. Ed 2019, 58, 2–11.

[52]. Sanchez-Cano C, Gianolio D, Romero-Canelon I, Tucoulou R, Sadler PJ, Chem. Commun 2019, 55, 7065–7068.

[53]. Xu Z, Kong D, He X, Guo L, Ge X, Liu X, Zhang H, Li J, Yang Y, Liu Z, Inorg. Chem. Front 2018, 5, 2100–2105.

[54]. Liu Z, Li J, Kong D, Tian M, Zhao Y, Xu Z, Gao W, Zhou Y, Eur. J. Inorg. Chem 2019, 287–294.

[55]. Zhang Y, Wen M-H, Qin G, Cai C, Chen T-Y, Metallomics 2022, 14, mfac087. [PubMed: 36367501]

[56]. Casey JR, Grinstein S, Orlowski J, Nat. Rev. Mol. Cell Biol 2010, 11, 50–61. [PubMed: 19997129]

[57]. Wang W, Zhao F, Ma X, Perry G, Zhu X, Mol. Neurodegener 2020, 15, 30. [PubMed: 32471464]

[58]. Federico A, Cardaioli E, Da Pozzo P, Formichi P, Gallus GN, Radi E, J. Neurol. Sci 2012, 322, 254–262. [PubMed: 22669122]

[59]. Chistiakov DA, Shkurat TP, Melnichenko AA, Grechko AV, Orekhov AN, Ann. Med 2018, 50, 121–127. [PubMed: 29237304]

[60]. Zhou B, Tian R, J. Clin. Invest 2018, 128, 3716–3726. [PubMed: 30124471]

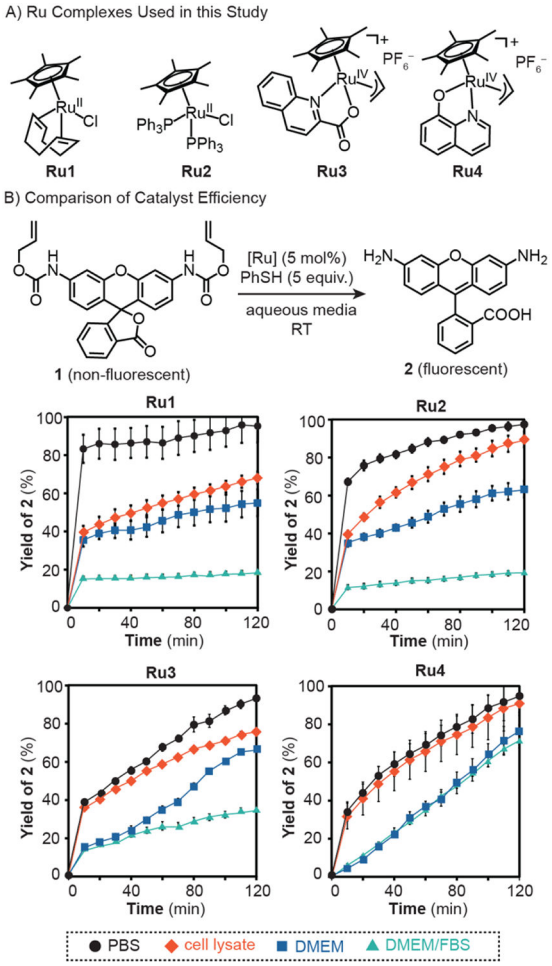

Figure 1.

A) Ru(II) and Ru(IV) complexes screened for their allylcarbamate cleavage efficiency. B) Fluorescence study of the conversion of **1** to **2** using various Ru complexes. Reaction conditions used: **1** (40 μM), PhSH (200 μM), and Ru catalysts (2 μM) in aqueous solvents. Yields were determined at λ_{em} = 522 nm (λ_{ex} = 450 nm) using a calibration curve. The data shown are the average of three independent experiments. PBS = phosphate-buffered saline, DMEM = Dulbecco's Modified Eagle Medium, FBS = fetal bovine serum. Triplicate experiments were performed with standard deviations typically <10%.

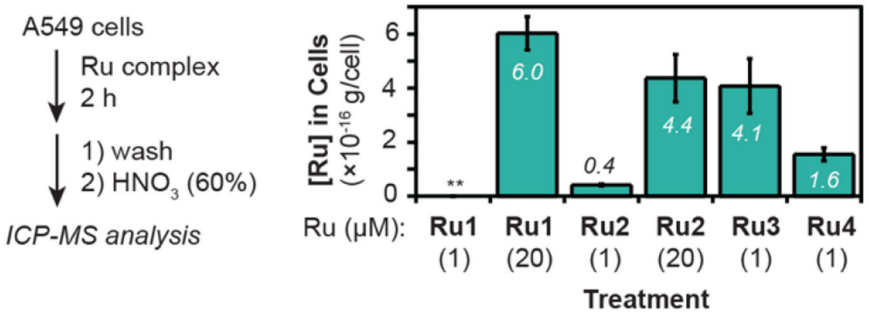

Figure 2.

Quantification of Ru uptake inside A549 cells after incubation with the complexes for 2 h. The Ru concentrations were measured using ICP-MS. The amount of Ru in cells treated with 1 μM of **Ru1** (marked with **) was below the detection limit. Experiments were performed in triplicate (see Table S2 for the full data and standard deviations).

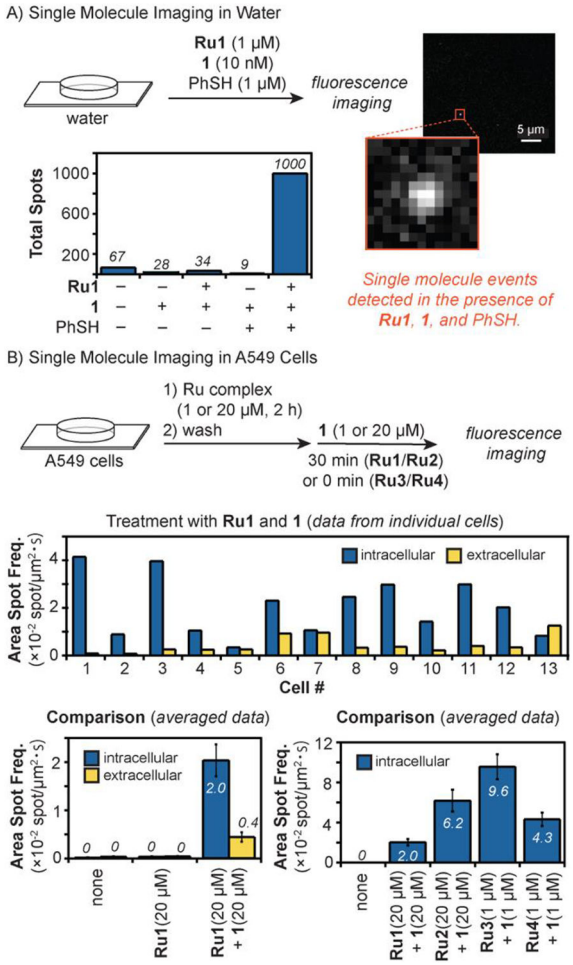

Figure 3.

A) Single-molecule fluorescence image and spot count obtained from the reaction of **Ru1**, **1**, and PhSH in water. B) Area spot frequency determined from the reaction of **1** and Ru complexes in A549 cells (n = ≥ 7 cells, see Figures S25-28 for the full data and standard deviations). These values are not normalized relative to the intracellular Ru concentration (see Figure S29 for Ru normalized data). Images were acquired in epi-fluorescence illumination mode. Imaging conditions used for both parts A and B: λ_{ex} = 488 nm, λ_{em} = 525 nm, speed = 10 fps, total time = 100 s.

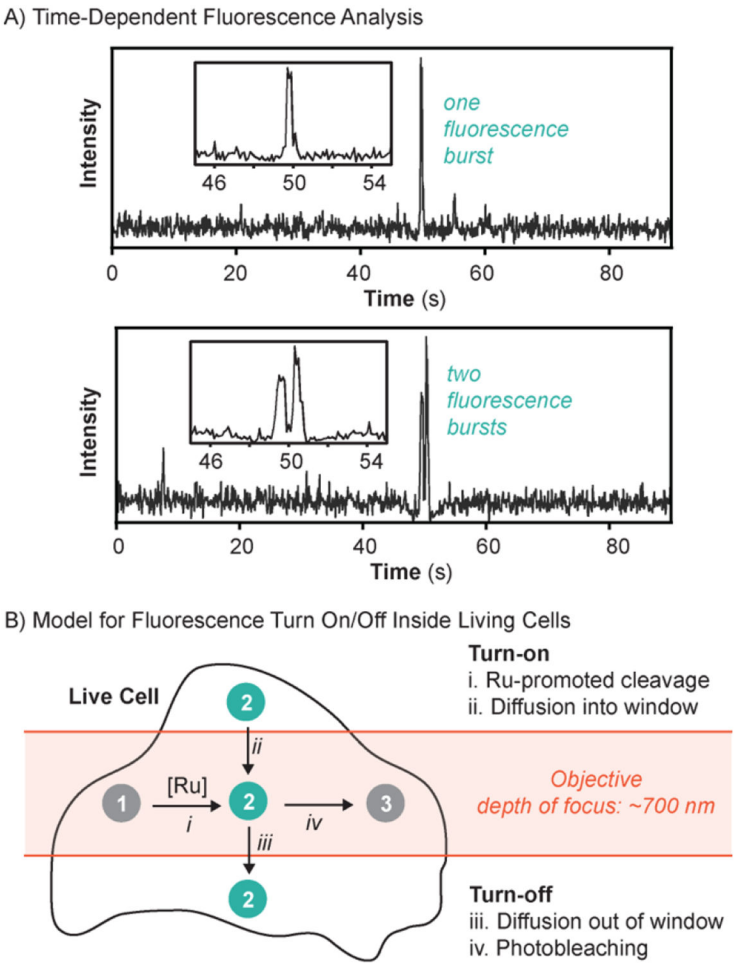

Figure 4.

A) Time-dependent fluorescence intensity of regions of interest (~7×7 pixels) containing single-molecule fluorescence bursts inside a cell. Cells were treated with Ru catalyst (20 μM) for 2 h, washed 3 times with FluoroBrite DMEM, and then treated with **1** (20 μM) for 30 min. B) Proposed model for the appearance and disappearance of fluorescence signals from live cell imaging studies. Compound **3** is a non-emissive photobleached product.

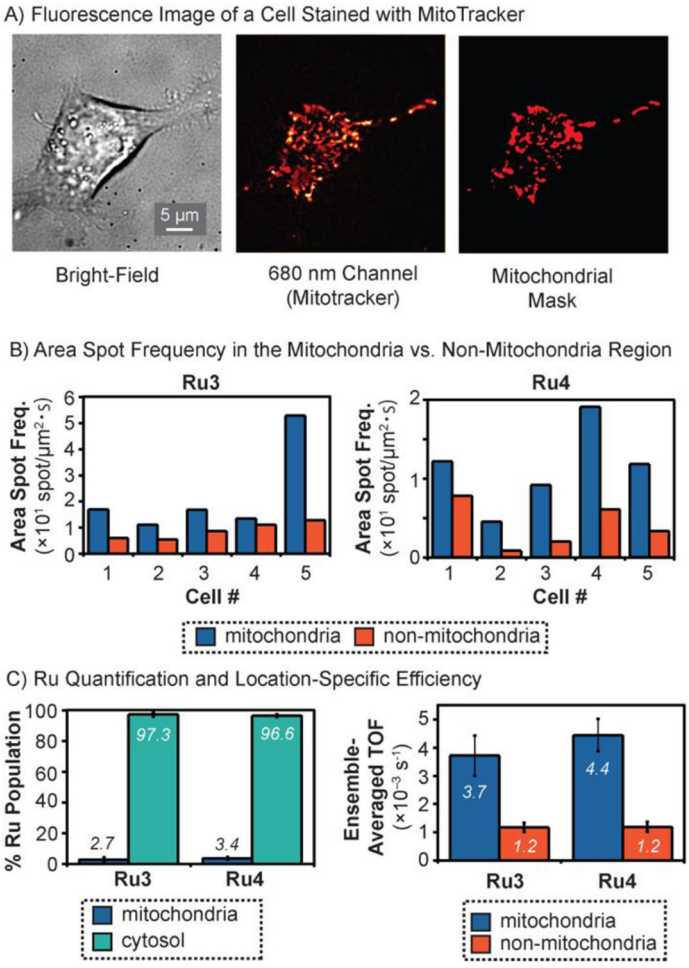

Figure 5.

A) Fluorescence image of an A549 cell stained with MitoTracker Deep Red. B) Comparison of the area spot frequency observed in the mitochondria vs. non-mitochondria regions in different cells treated with **1** and either **Ru3** or **Ru4**. Triplicate experiments were performed (see Table S3 for the full data and standard deviations); C) The percent population of Ru in the mitochondria vs. cytosol was determined by ICP-MS. An undetermined amount of Ru in the nuclei and cell debris may be lost due to the cell fractionation procedure. Mean and standard deviations were calculated using the spot frequency (Figure S27-28) and ICP-MS (Table S3) data.

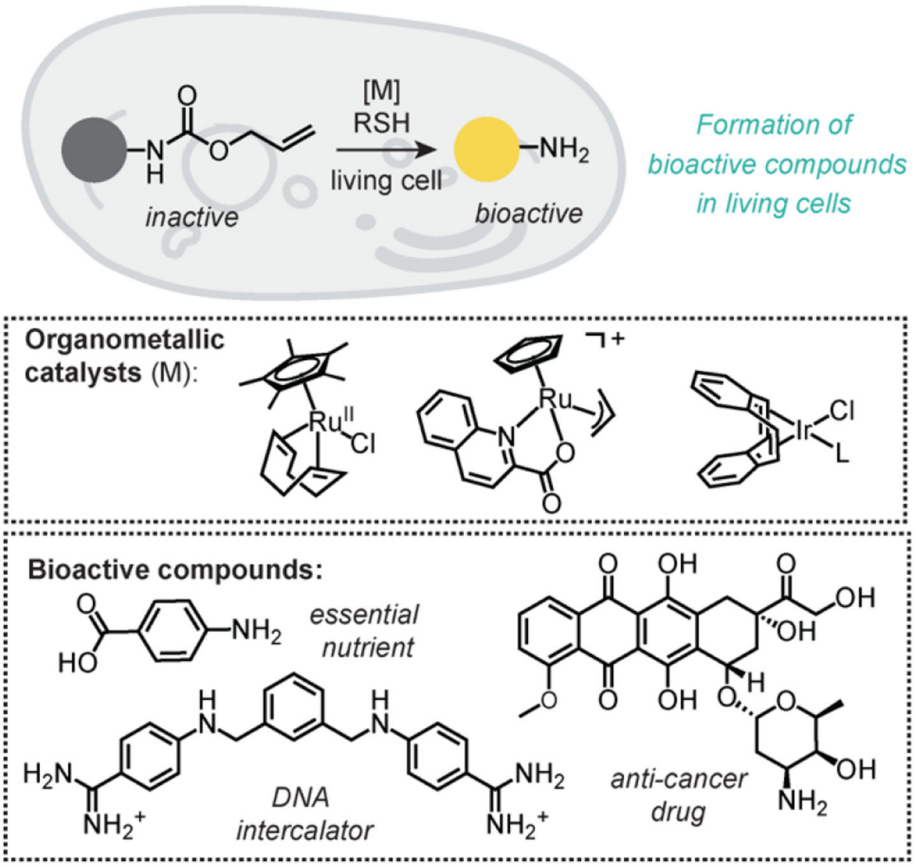

Scheme 1.

Allylcarbamate cleavage by organometallic catalysts inside living cells to form bioactive compounds.